Journal of Zhejiang University-SCIENCE A (Applied Physics & Engineering)
ISSN 1673-565X (Print); ISSN 1862-1775 (Online)
www.jzus.zju.edu.cn; www.springerlink.com
E-mail: jzus@zju.edu.cn

A load-holding time prediction method based on creep strain relaxation for the cold-stretching process of S30408 cryogenic pressure vessels*

Feng-qing XIAO[†1], Ying-zhe WU[†1], Jin-yang ZHENG[†‡1,2,3], Cun-jian MIAO[†4], Xiao-bo ZHU[1]

([1]*Institute of Process Equipment, Zhejiang University, Hangzhou 310027, China*)

([2]*High Pressure Process Equipment and Safety Engineering Research Center of Ministry of Education, Hangzhou 310027, China*)

([3]*State Key Laboratory of Fluid Power and Mechatronic Systems, Hangzhou 310027, China*)

([4]*Zhejiang Provincial Special Equipment Inspection and Research Institute, Hangzhou 310020, China*)

[†]E-mail: xiaofq@zju.edu.cn; yzwu@zju.edu.cn; jyzh@zju.edu.cn; miaocunjian@zju.edu.cn

Received Dec. 30, 2016; Revision accepted Apr. 14, 2017; Crosschecked Oct. 11, 2017

Abstract: Austenitic stainless steel (ASS) has been widely used for cryogenic pressure vessels. Its high strain hardening characteristic allows cold-stretching. In the cold-stretching process, the load-holding time is a critical operating parameter which affects the final deformation of the material. In this paper, a load-holding time prediction method for the cold-stretching process of S30408 cryogenic pressure vessels is proposed, based on room-temperature creep strain relaxation. The proposed correlation has only one variable, the maximum circumferential stress applied to the cylindrical shell, which can be easily obtained by finite element analysis. Consequently, the strain rate measurement during the cold-stretching process is significantly simplified. The prediction method and the strain rate measurement were verified by experimental measurements conducted on two vessels manufactured via the cold-stretching process. The measured strain relaxation times accurately matched the calculated values and the load-holding time for the process was well predicted.

Key words: Cold-stretching; Room-temperature creep (RTC); Austenitic stainless steel (ASS); Cryogenic vessels
http://dx.doi.org/10.1631/jzus.A1600798 **CLC number:** TH49

1 Introduction

Austenitic stainless steel (ASS) has been widely used for cryogenic pressure vessels due to its excellent mechanical performance at low temperatures (Zheng *et al*., 2009; Miao *et al*., 2013). However, in the design of ASS products the allowable stress is low because of the relatively low yield strength of ASS (Zheng *et al*., 2011). On the other hand, ASS exhibits high strain hardening, which allows cold-stretching to raise the yield strength of the material, enabling an increase in the allowable design stress of cryogenic pressure vessels (see EN 13458-2-2002 (CEN, 2002) and ASME BPVC VIII-1 (ASME, 2015)).

The cold-stretching procedure consists of three steps: (1) an uploading phase, in which the pressure is linearly increased up to cold-stretching load, and a corresponding plastic strain occurs, shown as *O*–*A* in Fig. 1; (2) a load-holding phase, in which the pressure maintains a constant value, and the material experiences a creep deformation, shown as *A*–*B* in Fig. 1; (3) an off-loading phase, in which the pressure is unloaded, and the cold-stretching is completed, shown as *B*–*C* in Fig. 1. The load-holding time, i.e.,

‡ Corresponding author

* Project supported by the National Key Research and Development Program of China (No. 2016YFC0801905)

ORCID: Feng-qing XIAO, http://orcid.org/0000-0003-4698-8838

© Zhejiang University and Springer-Verlag GmbH Germany 2017

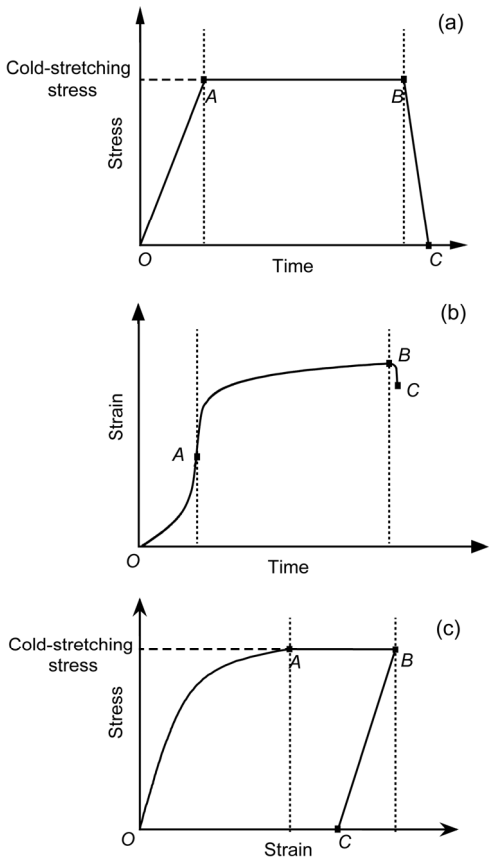

Fig. 1 Three phases of the cold-stretching process for cryogenic pressure vessels: (a) stress vs time; (b) strain vs time; (c) stress vs strain

the time until the strengthening pressurization is terminated, is a critical operation parameter to control because it affects the final deformation of the material after the stretching process. However, the load-holding time is unknown prior to the cold-stretching operation, as it is determined by the strain rate measured during the process. In practice, the strain rate measurement is complicated, and consumes significant time and human resources, particularly for large vessels or a large number of products. Thus, a method to predict accurately the required loading time prior to the cold-stretching operation is desired. Moreover, for practical reasons, the strain rate measurement needs to be further simplified to reduce production costs.

To predict the load-holding time, the detailed deformation behavior of ASS was investigated. During the load-holding phase of the cold-stretching process, a post-yielding stress is applied on a vessel due to the controlled constant cold-stretching pressure, causing permanent deformation due to tension and creep (Zheng *et al.*, 2009; 2011). During the pressure-holding phase, as the cold-stretching process is performed at room temperature, which is much lower than the temperature required to trigger thermal softening, the strain ε_c of the ASS increases logarithmically (Fig. 1b), corresponding to the primary stage in the typical three-stage creep law (Schoeck, 1961). In this phase, the strain increases continuously with a dropping growth rate, while the applied stress is constant. Strain relaxation is achieved as the strain rate approaches zero, resulting in termination of creep or in an equilibrium minimum creep if there is a relatively high stress level, which eventually results in a steady-state creep.

Although metal creep at a relatively high temperature has been investigated thoroughly (Lim *et al.*, 2013; Li and Xu, 2016), room-temperature creep (RTC) has rarely been discussed. Kassner *et al*. (2011) conducted experimental research on AISI 304 and found significant creep plasticity at room temperature. Krempl (1979) carried out a series of tensile tests on AISI 304 at various strain rates, and showed significant rate-sensitivity, creep, and relaxation. Wang S.H. *et al*. (2001), Bao *et al*. (2015), and Wang Y.Q. *et al*. (2015) studied creep deformation and the effect of strain rate on the stress-strain behavior of several steels at room temperature. Independent of yielding behavior, significant post-yield creep deformation was observed. This was attributed to the glide of existing dislocations mobilized under creep stress, and new mobile dislocations generated due to plastic deformation in the loading process. However, the phenomenon of RTC during the cold-stretching process has never been studied. Furthermore, the existing classic creep rate equation involves several microscopic parameters, such as the number of dislocation segments per unit volume, the frequency of dislocation loop vibrations, and the activation energy. The classic equation is useful for explaining the mechanism of RTC, but is impractical for engineering purposes.

Therefore, in this study we investigated the RTC of S30408. The parameters that respond to the creep strain rate and the strain relaxation time were obtained experimentally. Based on the strain relaxation, the load-holding time for the cold-stretching process can be predicted as a function of the maximum applied stress. Based on this prediction method, the strain rate measurement for the cold-stretching

operation can be simplified. The prediction method was experimentally verified and the simplified measurement validated.

2 Strain relaxation time

2.1 Strain rate of the logarithmic creep

The strain rate due to the RTC phenomenon is critical in determining the strain relaxation time. Based on the logarithmic time law, the RTC strain is given by Schoeck (1961) as

$$\varepsilon_{\mathrm{RTC}} = \alpha \ln\left(1+\frac{t}{\tau}\right), \tag{1}$$

where t is the creep time, τ is a characteristic time, which was found to depend very little on the temperature (Davis and Thompson, 1950), and α is a dimensionless coefficient, which is strongly related to the material, temperature, and coefficient of work hardening (Schoeck, 1961). Given a constant uploading rate on S30408 at room temperature in this study, the dependencies of α on the material and temperature were eliminated, while the coefficient of work hardening could be fully determined by the stress level (Feng, 1999; Boyle and Spence, 2013). Consequently, α was expected to be a function of the applied stress. α and τ were determined experimentally via uniaxial creep testing in tension for the ASS.

Then, the RTC strain rate can be calculated by

$$\dot{\varepsilon}_{\mathrm{RTC}} = \frac{\partial \varepsilon_{\mathrm{RTC}}}{\partial t} = \frac{\alpha}{\tau + t}. \tag{2}$$

2.2 Uniaxial creep tests in tension

The creep tests were performed on an industrial manufactured S30408 in as-received condition. The tested S30408 material was a hot-rolled and solution heat-treated plate with a thickness of 12 mm. Its chemical composition is listed in Table 1, along with the requirements specified in Chinese standard GB 24511 (AQSIQ, 2009). According to the Chinese standards GB/T 2039 (AQSIQ, 2012) and GB/T 228.1 (AQSIQ, 2010), cylindrical tensile specimens were machined from the plate with their axis along the hot-rolling direction. The nominal dimensions of the specimen in the gauge section were 25 mm (length)× 5.0 mm (diameter) (Fig. 2). The creep tests were carried out on an MTS 810-250 kN universal testing machine with a load accuracy below 0.5%. The strain was measured by a calibrated MTS 632.53F-14 extensometer with an accuracy of ±1% Rd from 2% to 100% of the range. The Mandatory Appendix 44 of ASME (2015) suggests a cold-stretching pressure of 1.5–1.6 times the design pressure (1.5 times suggested by CEN (2002)), corresponding to a cold-stretching stress σ of 405–432 MPa for S30408 steel. Considering the minimum yield strength and the minimum ultimate tensile strength of S30408 suggested in GB 24511 (AQSIQ, 2009), the creep tests were performed at nine stress levels: 260, 310, 350, 370, 390, 410, 460, 530, and 560 MPa. Furthermore, the application of the test force should be as rapid as possible for creep testing, as suggested in ISO 204-2009 (ISO, 2009). However, in this study, the applied stress rate was controlled at 40 MPa/min for all tests, which is an uploading speed commonly used during a cold-stretching procedure.

The measured creep strain versus the time at different stress levels is presented in Fig. 3. For low

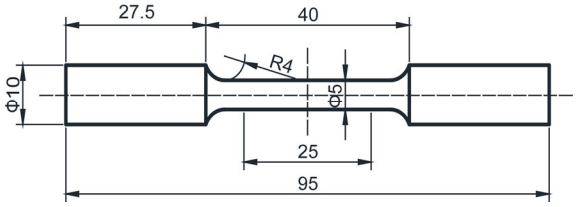

Fig. 2 Schematic illustration of tensile specimen (unit: mm)

Table 1 Chemical composition of materials for creep tests

Source	Chemical composition (%, in weight)							
	C	Si	Mn	P	S	Ni	Cr	N
Tested S30408	0.06	0.67	1.41	0.023	0.006	8.27	18.16	0.029
Specification of GB 24511 (AQSIQ, 2009)	≤0.08	≤0.75	≤2.00	≤0.035	≤0.02	8–10.5	18–20	≤0.10

stress levels (260–310 MPa), which are still in the elastic range, the RTC strain was limited and declined to a zero strain rate after about 2000 s. However, the RTC phenomenon became significant as the stress increased. Meanwhile, the strain continued to rise with time, even when the stress was kept constant. All curves perfectly followed the logarithmic relationship, and were fitted individually, based on Eq. (1). The fitted α and τ are listed in Table 2 along with the R-squared and the root mean squared errors (RMSEs) of the fittings.

As mentioned in Section 2.1, α and τ were expected to be functions of the stress in this study, where the material, the temperature, and the uploading rate were fixed. To find such relationships, fitted α and τ were plotted against the stress (Figs. 4a and 4b, respectively). As shown in Fig. 4a, the change in the fitted α was approximately linear against the stress, with the linear correlation given by

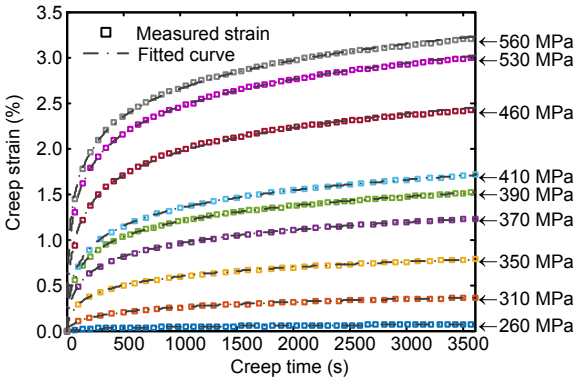

Fig. 3 Strains at variety of stress levels in the uniaxial creep testes

Table 2 Fitting results for the strains measured in the uniaxial creep tests based on the logarithmic time law

Stress level (MPa)	α (%)	τ (s)	R-squared	RMSE (%)
260	0.0206	148.660	0.9718	0.026
310	0.0838	48.841	0.9993	0.019
350	0.1480	18.343	0.9996	0.029
370	0.2142	11.614	1.0000	0.014
390	0.2500	8.371	0.9998	0.036
410	0.2872	9.423	0.9999	0.027
460	0.3805	5.787	0.9977	0.176
530	0.4361	3.600	0.9990	0.136
560	0.4493	2.734	0.9980	0.198

$$\alpha_{\text{fitted}}(\sigma)=1.521\times10^{-3}\sigma-0.363. \tag{3}$$

The characteristic time τ basically is the order of the duration of the extension on loading (Nabarro, 2001). Based on the creep tests, the fitted τ decreased rapidly as the stress level rose (Fig. 4b), and the following power correlation was found:

$$\tau_{\text{fitted}}(\sigma)=4.912\times10^{7}(\sigma-1.707\times10^{2})^{-2.828}. \tag{4}$$

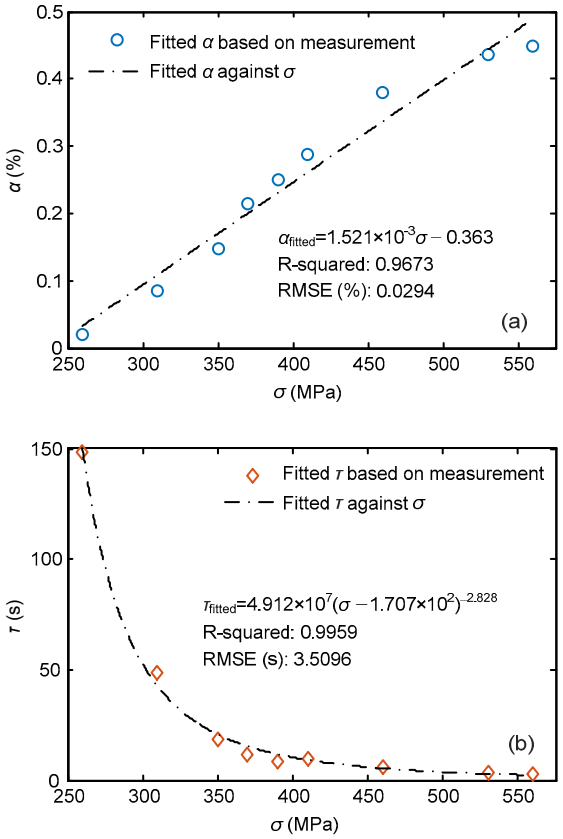

Fig. 4 Correlations of α–σ (a) and τ–σ (b)

2.3 Strain relaxation time calculations

Substituting Eqs. (3) and (4) into Eq. (2), the strain rate due to RTC can be expressed as a percentage as

$$\dot{\varepsilon}_{\text{RTC}}(\sigma)=\frac{\alpha(\sigma)}{\tau(\sigma)+t}=\frac{1.521\times10^{-3}\sigma-0.363}{4.912\times10^{7}(\sigma-1.707\times10^{2})^{-2.828}+t}. \tag{5}$$

Fig. 5 plots the strain rate variation as a function of time for different stress levels. The dashed line represents a strain rate of 0.1 %/h, which is suggested by the Mandatory Appendix 44 of ASME (2015) and CEN (2002) as the strain relaxation criterion. The time intersection of the strain rate curve to the 0.1 %/h criterion is therefore the strain relaxation time, which rapidly increased as the stress increased. By substituting the 0.1 %/h strain rate criterion into Eq. (5) and re-arranging, the strain relaxation time can be expressed in minutes as

$$t_{sr}(\sigma)=\frac{1}{60}\left[\frac{\alpha(\sigma)}{\dot{\varepsilon}_{\mathrm{RTC,\,cr}}}-\tau(\sigma)\right], \tag{6}$$

where $\dot{\varepsilon}_{\mathrm{RTC,\,cr}}$ is the strain relaxation criterion. The characteristic time $\tau(\sigma)$ at the stress range of interest (Table 2), was usually much shorter than the resultant strain relaxation time. Thus, it can be neglected to obtain a simpler correlation, and Eq. (6) becomes

$$\begin{aligned} t_{sr}(\sigma)&=\frac{1}{60}\frac{\alpha(\sigma)}{\dot{\varepsilon}_{\mathrm{RTC,\,cr}}}\\ &=\frac{1}{60}\cdot\frac{1.521\times10^{-3}\sigma-0.363}{0.1/3600}\\ &=0.9126\sigma-217.8. \end{aligned} \tag{7}$$

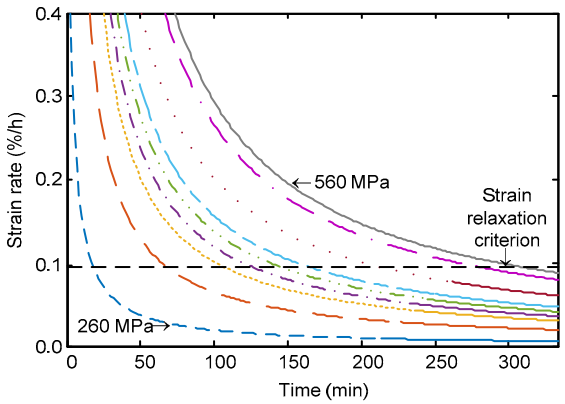

Fig. 5 Calculated creep strain rate as a function of time at different stress levels

The load-holding time (t_{hold}) of the cold-stretching process was determined based on the strain relaxation of the material, and in consideration of practical applications: the time should be no less than 30 min, and the maximum circumferential strain rate requirement of 0.1 %/h should be met during the last 15 min. To meet the second requirement, solving the following equation (expressed in minutes):

$$\frac{1}{15}\int_{t_{\mathrm{hold}}-15}^{t_{\mathrm{hold}}}\dot{\varepsilon}_{\mathrm{RTC}}\mathrm{d}t=\dot{\varepsilon}_{\mathrm{RTC,\,cr}} \tag{8}$$

yields

$$t_{\mathrm{hold}}=15\left[1-\exp\left(\frac{-15\dot{\varepsilon}_{\mathrm{RTC,\,cr}}}{\alpha(\sigma_{\mathrm{k,max}})}\right)\right]^{-1}, \tag{9}$$

where $\sigma_{\mathrm{k,max}}$ is the maximum circumferential stress on the vessel.

Therefore, the load-holding time can be conservatively calculated in minutes as

$$t_{\mathrm{hold}}(\sigma_{\mathrm{k,max}})=\max\left\{30,\frac{15}{1-\exp\left[(14.52-0.0608\sigma_{\mathrm{k,max}})^{-1}\right]}\right\}. \tag{10}$$

The load-holding time calculated by Eq. (10) is plotted against the maximum circumferential stress in Fig. 6. Eq. (10), including only one variable $\sigma_{\mathrm{k,max}}$, is convenient for predicting the load-holding time.

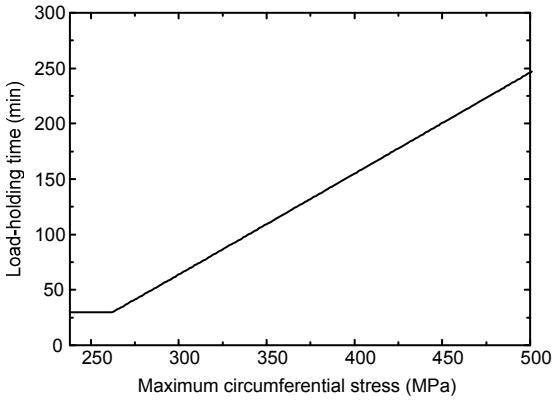

Fig. 6 Predicted load-holding time as a function of the maximum circumferential stress

3 Experimental verification

3.1 Sample vessels

To validate the strain relaxation time prediction method described in Section 2, the finite element (FE)

simulations and experimental measurements were conducted on the cold-stretching process for two cryogenic pressure vessels made of standard S30408, denoted as vessels A and B (Fig. 7). Both vessels had ellipsoidal heads. Vessel A with a design pressure of 1.80 MPa, had a diameter of 1500 mm, total length of 4400 mm, and design thickness of 6.0 mm. Its cylindrical shell consisted of three segments welded together. A manhole nozzle and backing plates were designed as shown in Fig. 7a.

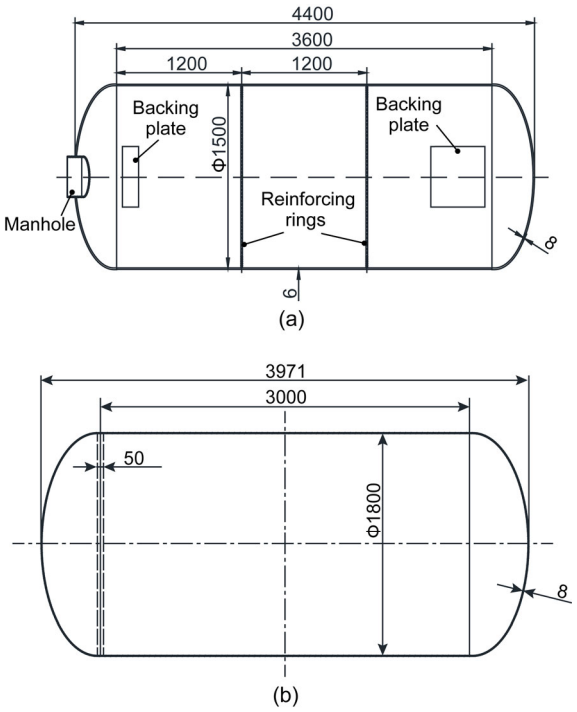

Fig. 7 Main structural parameters of vessels A (a) and B (b) (unit: mm)

3.2 Maximum stress level and strain rate measurement simplification

Since the strain relaxation time is positively related to the stress, the maximum stress level under the cold-stretching pressure should be found to obtain a conservative load-holding time, which represents the structural stability of the entire vessel. The stress distribution on the vessel can be found by FE simulation prior to the cold-stretching process, and consequently the maximum stress level can be determined.

During the cold-stretching process, the strain rate monitoring was based on a real-time measurement of the change in the circumference of the cylindrical shell. The measurement gives an average strain rate around the cylindrical shell, and consequently an average stress level is more reasonable for selecting as the input for Eq. (9).

A nonlinear analysis was performed based on the geometries of the two vessels and the applied cold-stretching pressure. The bilinear isotropic hardening model was used, which is applicable to large strain analysis. The analysis was based on the true stress-strain curves of the S30408. FE simulations were conducted to model the uploading phase of the cold-stretching process. The stress and strain states of the vessel at the end of the uploading phase were calculated.

The resultant von Mises equivalent stress distributions on the two vessels are presented in Fig. 8. Generally, large stress occurred in the middle of the cylindrical shell segments. Also, stress was concentrated at positions where the structure was discontinuous, such as the root position of the manhole nozzle and the area around the backing plate, as shown in Fig. 8a for vessel A. However, these stress concentrations were not taken into account, because the factor determining the strength of such a thin-shell vessel is the circumferential stress at the cylindrical shell, rather than the stress concentration at localized structural discontinuities.

Several measuring positions denoted as Sn (n=1, 2, …) were selected where large circumferential average stress occurred (Fig. 9). The average stress values are also presented in Fig. 9. For vessel A, the maximum circumferential average stress of 336.64 MPa occurred at S1. The stress distribution was more uniform for vessel B due to its simple and symmetric geometry, and the maximum circumferential average stress of 387.43 MPa was found at S4. Thus, the cold-stretching process could be greatly simplified by measuring only S1 for vessel A and S4 for vessel B. Such simplification is very practical and reduces the production cost, particularly for the production of large vessels or a large number of products.

Nevertheless, for the experimental verification, the circumference at all of those positions was measured. Based on those measurements, the corresponding

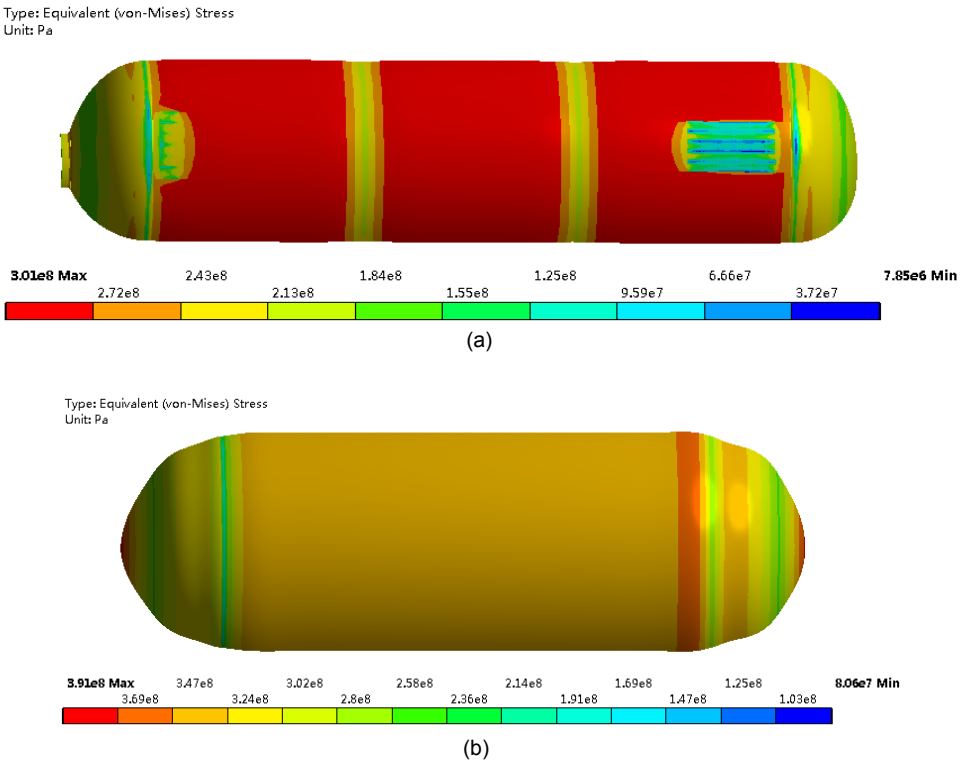

Fig. 8 Equivalent stress distribution on the vessels after the uploading process of vessels A (a) and B (b)

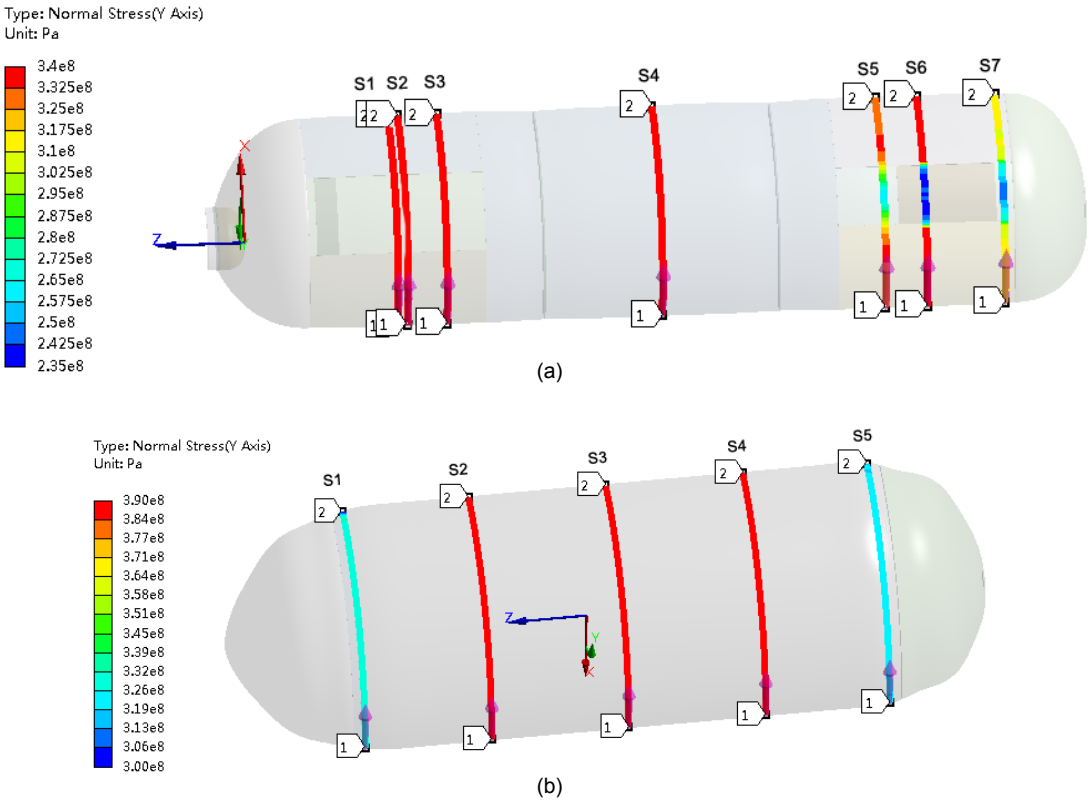

Fig. 9 Measuring positions, simulated stress distributions, and average circumferential stresses of vessels A (a) and B (b)

strain relaxation times were found and compared with the predicted values.

3.3 Experimental verification

The cold-stretching process followed the standard procedure suggested by the Mandatory Appendix 44 of ASME BPVC VIII-1 (ASME, 2015) and EN 13458-2-2002 (CEN, 2002). Thus, the cold-stretching pressure was 2.70 MPa for vessel A and 3.45 MPa for vessel B. The uploading rate was held constant at 40 MPa/min during the cold-stretching process. The pressure was raised up to the design pressure, and then a safety check was made before it was increased further to the cold-stretching pressure. The load-holding phase lasted with a constant load until the strain was relaxed, i.e., $t_{sr}\geq 30$ min or $\dot{\varepsilon} < 0.1\%/\text{h}$ for the last 15 min. The circumferences at the selected measuring positions (Fig. 9) were measured and recorded every 5 min during the cold-stretching process. Fig. 10 shows the photos of the field measurement set up for the two vessels.

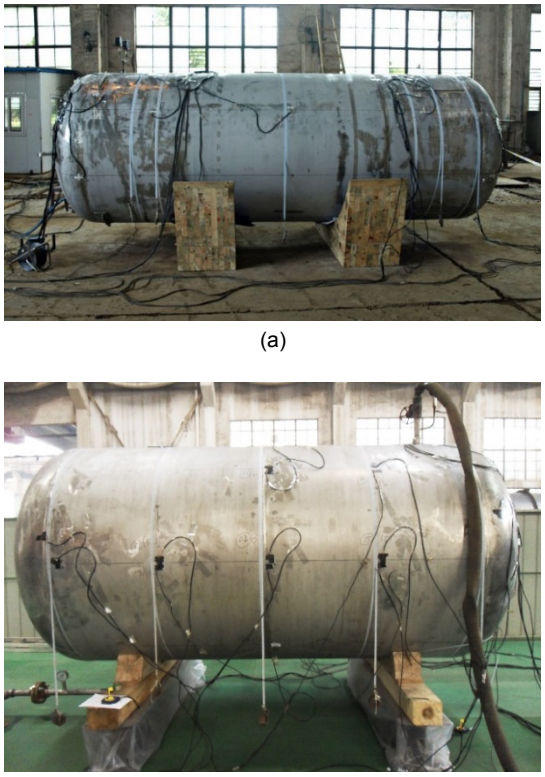

(a)

(b)

Fig. 10 Testing field photos of the cold-stretching process for vessels A (a) and B (b)

The measured average circumferential strains and the strain rates are presented in Fig. 11. For vessel A, the maximum stresses occurred at S1, S2, and S3. The measured strains at these positions were quite similar, and larger than those at other positions, as expected. The strains at other positions also reached relaxation after a long time (85 min). Similar strain behavior was found for vessel B, which had a higher stress level and consequently strain relaxation times of up to 120 min.

The strain relaxation times at the measuring positions were calculated using Eq. (9), and compared with the measured values in Table 3. The relative errors of the calculated strain relaxation times were generally less than 15%, and the absolute average error was 7.53%. Furthermore, most of the errors were positive, which means that the calculation is normally conservative. Based on the maximum stresses of two vessels, the predicted load-holding times were 97.07 min for vessel A and 143.41 min for vessel B. As shown in Figs. 11a and 11b, the predicted load-holding times can indicate when the vessel material is strain relaxed and when its geometry is stable.

4 Conclusions

In this paper, a load-holding time prediction method for the cold-stretching process of S30408 cryogenic pressure vessels is proposed. Based on the room-temperature creep of ASS during the load-holding phase, the strain and its change rate are evaluated as a function of time by a classical logarithmic time law for creep. Two critical parameters α and τ in the strain rate correlation were identified to be related to the stress level within the material. Uniaxial creep tests in tension for S30408 stainless steel were carried out to determine the correlation of α and τ against the stress. According to the strain rate criterion for strain relaxation suggested by ASME and CEN industrial standards, an equation for calculating the strain relaxation time of S30408 was devised. A correlation for predicting the load-holding time of the cold-stretching process was generated based on the strain relaxation feature of S30408. The proposed predictive correlation has only one macroscopic variable, the maximum circumferential stress applied on

Table 3 Comparison between the measured and calculated strain relaxation times at the measuring positions

Vessel	Measuring position	$\sigma_{c,avg}$ (MPa)	Loading time, t_{sr} (min)		Relative error (%)
			Measured	Calculated	
A	S1	336.64	95	97.07	2.17
	S2	336.47	95	96.94	2.04
	S3	336.27	90	96.81	7.56
	S4	329.80	95	96.70	1.78
	S5	311.71	85	90.90	6.95
	S6	296.50	80	74.45	−6.94
	S7	336.60	55	60.64	10.26
B	S1	314.23	70	82.57	9.62
	S2	379.64	120	143.37	13.59
	S3	379.67	120	143.40	13.61
	S4	379.68	120	143.41	13.62
	S5	321.29	85	89.13	−2.16

$\sigma_{c,avg}$ is the average circumferential stress on measuring position Sn

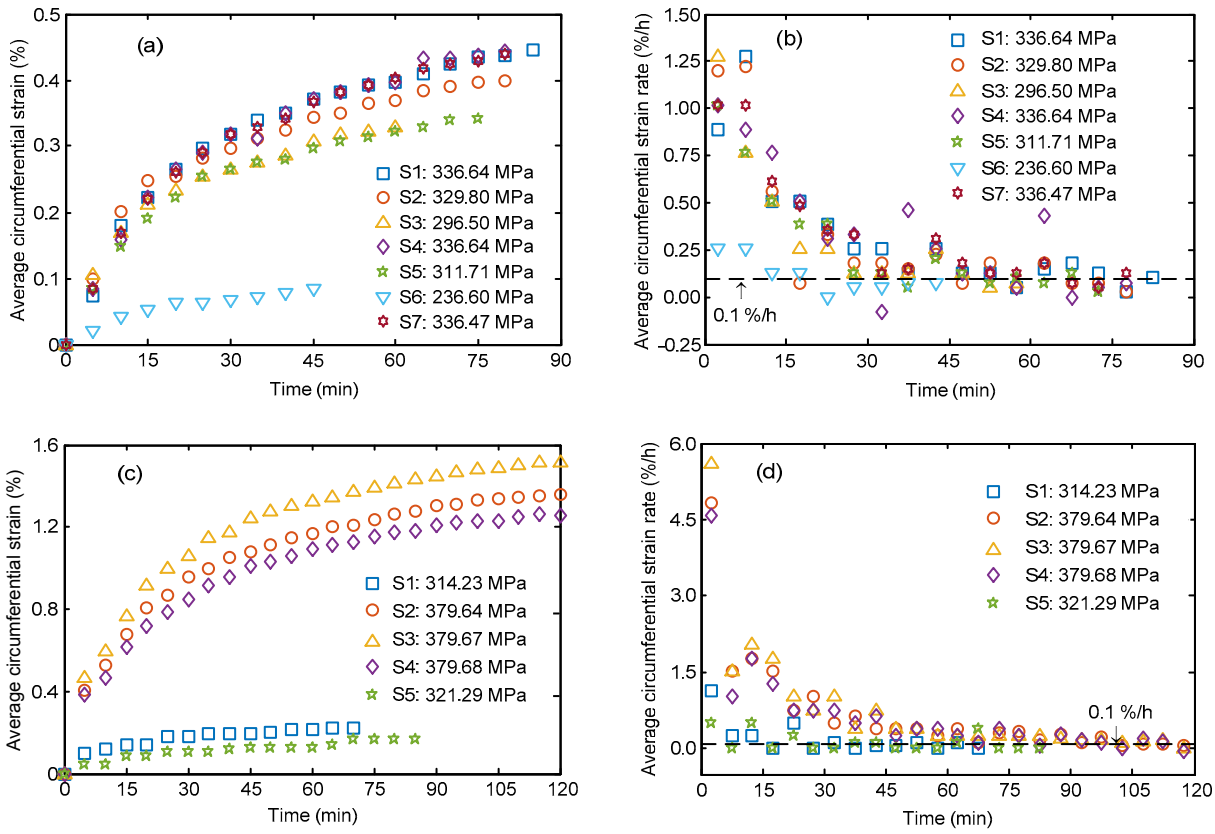

Fig. 11 Measured circumferential strains and strain rates: strains (a) and strain rates (b) for vessel A; strains (c) and strain rates (d) for vessel B

the cylindrical shell. Thus, the strain rate measurement during the cold-stretching operation is significantly simplified by setting the measuring position only at the point on the circumference where the maximum circumferential stress is found by FE analysis. Finally, the load-holding time prediction equation and the simplified strain rate measuring method were verified by experiments conducted on

two vessels manufactured via the cold-stretching operation. The measured strain relaxation times matched calculated values accurately and the load-holding time for the process was well predicted.

References

AQSIQ (General Administration of Quality Supervision, Inspection and Quarantine of the People's Republic of China), 2009. Stainless Steel Plate, Sheet and Strip for Pressure Equipments, GB 24511-2009. Standardization Administration of the People's Republic of China, Beijing, China (in Chinese).

AQSIQ (General Administration of Quality Supervision, Inspection and Quarantine of the People's Republic of China), 2010. Metallic Materials—Tensile Testing—Part 1: Method of Test at Room Temperature, GB/T 228.1-2010. Standardization Administration of the People's Republic of China, Beijing, China (in Chinese).

AQSIQ (General Administration of Quality Supervision, Inspection and Quarantine of the People's Republic of China), 2012. Metallic Materials—Uniaxial Creep Testing Method in Tension, GB/T 2039-2012. Standardization Administration of the People's Republic of China, Beijing, China (in Chinese).

ASME (American Society of Mechanical Engineers), 2015. Boiler and Pressure Vessel Code VIII, Division 1: Rules for Construction of Pressure Vessels, ASME BPVC VIII. ASME, New York, USA.

Bao, G.H., Chen, Y., Ma, J.E., *et al.*, 2015. Microstructure and properties of cold drawing Cu-2.5% Fe-0.2% Cr and Cu-6% Fe alloys. *Journal of Zhejiang University-SCIENCE A (Applied Physics & Engineering)*, **16**(8): 622-629. http://dx.doi.org/10.1631/jzus.A1400285

Boyle, J.T., Spence, J., 2013. Stress Analysis for Creep. Butterworth & Co., London, UK.

CEN (The European Committee for Standardization), 2002. Cryogenic Vessels—Static Vacuum Insulated Vessels, EN 13458-2-2002. CEN, Brussels, Belgium.

Davis, M., Thompson, N., 1950. Creep in a precipitation-hardened alloy. *Proceedings of the Physical Society. Section B*, **63**(11):847-866. http://dx.doi.org/10.1088/0370-1301/63/11/303

Feng, D., 1999. Metal Physics: Metal Mechanical Property (Vol. 3). Science Press, Beijing, China (in Chinese).

ISO (International Organization for Standardization), 2009. Metallic Materials—Uniaxial Creep Testing in Tension—Method of Test, ISO 204-2009. International Organization for Standardization, Geneva, Switzerland.

Kassner, M.E., Geantil, P., Rosen, R.S., 2011. Ambient temperature creep of type 304 stainless steel. *Journal of Engineering Materials and Technology*, **133**(2):021012. http://dx.doi.org/10.1115/1.4003110

Krempl, E., 1979. An experimental study of room-temperature rate-sensitivity, creep and relaxation of AISI type 304 stainless steel. *Journal of the Mechanics and Physics of Solids*, **27**(5-6):363-375. http://dx.doi.org/10.1016/0022-5096(79)90020-6

Li, H.D., Xu, S.L., 2016. Rate dependence of ultra high toughness cementitious composite under direct tension. *Journal of Zhejiang University-SCIENCE A (Applied Physics & Engineering)*, **17**(6):417-426. http://dx.doi.org/10.1631/jzus.A1600031

Lim, J.S., Kim, T.S., Kim, S.H., 2013. Ultimate strength of single shear bolted connections with cold-formed ferritic stainless steel. *Journal of Zhejiang University-SCIENCE A (Applied Physics & Engineering)*, **14**(2):120-136. http://dx.doi.org/10.1631/jzus.A1100316

Miao, C.J., Zheng, J.Y., Gao, X.Z., *et al.*, 2013. Investigation of low-cycle fatigue behavior of austenitic stainless steel for cold-stretched pressure vessels. *Journal of Zhejiang University-SCIENCE A (Applied Physics & Engineering)*, **14**(1):31-37. http://dx.doi.org/10.1631/jzus.A1200140

Nabarro, F.R.N., 2001. The time constant of logarithmic creep and relaxation. *Materials Science and Engineering: A*, **309-310**: 227-228. http://dx.doi.org/10.1016/S0921-5093(00)01692-0

Schoeck, G., 1961. Mechanical Behaviour of Materials at Elevated Temperature. McGraw–Hill, New York, USA.

Wang, S.H., Zhang, Y.G., Chen, W.X., 2001. Room temperature creep and strain-rate-dependent stress-strain behavior of pipeline steels. *Journal of Materials Science*, **36**(8): 1931-1938.

Wang, Y.Q., Liao, X.W., Zhang, Y.Y., *et al.*, 2015. Experimental study on the through-thickness properties of structural steel thick plate and its heat-affected zone at low temperatures. *Journal of Zhejiang University-SCIENCE A (Applied Physics & Engineering)*, **16**(3): 217-228. http://dx.doi.org/10.1631/jzus.A1400273

Zheng, J.Y., Miao, C.J., Shou, B.N., 2009. Light-weight: a trend in the development of pressure vessels. *Pressure Vessel Technology*, **26**(9):42-48 (in Chinese).

Zheng, J.Y., Guo, A.B., Miao, C.J., *et al.*, 2011. Cold stretching of cryogenic pressure vessels from austenitic stainless steels. ASME 2011 Pressure Vessels and Piping Conference, p.693-698. http://dx.doi.org/10.1115/PVP2011-57331

中文概要

题　目：一种基于蠕变应变弛豫的S30408深冷容器应变强化保载时间预测方法

目　的：奥氏体不锈钢（ASS）在深冷压力容器中应用广泛。ASS较高的应变硬化特性有助于其产生应变

强化。在应变强化过程中，保载时间是影响材料最终变形量的关键参数。基于室温蠕变应变弛豫理论，本文旨在提出一种S30408深冷压力容器应变强化过程中的保载时间预测方法。

创新点： 1. 根据室温蠕变应变弛豫理论，保载过程即为材料在室温蠕变中应变速率逐渐减缓、材料结构逐渐稳定的过程；本文据此获得了保载时间的计算模型。2. 结合材料试验与容器试验，将计算模型中涉及的多个微观变量转换为唯一宏观变量——圆柱壳上的最大环向应力，可为常规工业生产提供定量的、具有实际可操作性的技术支持。

方　法： 1. 根据室温蠕变应变弛豫理论，建立蠕变本构关系，得出保载时间计算模型。2. 通过材料试验，考虑实际生产中的特定条件，将保载时间计算模型的多个微观变量简化为唯一宏观变量。3. 通过在多个工业规模的容器上进行实验，比较验证所提计算方法的可靠性。

结　论： 1. 室温蠕变应变弛豫理论可以用于描述应变强化保载过程中的材料变化。2. 容器保载时长，即材料应变弛豫时长，与其所承受的最大应力有关。3. 所提出的保载时间计算方法可以为容器保载时间提供可靠预测；其平均绝对误差为7.53%，且绝大部分情况下偏于保守。

关键词： 应变强化；室温蠕变；奥氏体不锈钢；深冷容器